Neuron
Article

A Sensorimotor Role for Traveling Waves in Primate Visual Cortex

Theodoros P. Zanos,[1,*] Patrick J. Mineault,[1,2] Konstantinos T. Nasiotis,[1] Daniel Guitton,[1] and Christopher C. Pack[1,*]
[1]Montreal Neurological Institute, McGill University, 3801 University Ave, #896, Montreal, QC H2V2A1, Canada
[2]Department of Neurobiology, David Geffen School of Medicine, University of California, Los Angeles, CA 90095, USA
*Correspondence: theodoros.zanos@mcgill.ca (T.P.Z.), christopher.pack@mcgill.ca (C.C.P.)
http://dx.doi.org/10.1016/j.neuron.2014.12.043

SUMMARY

Traveling waves of neural activity are frequently observed to occur in concert with the presentation of a sensory stimulus or the execution of a movement. Although such waves have been studied for decades, little is known about their function. Here we show that traveling waves in the primate extrastriate visual cortex provide a means of integrating sensory and motor signals. Specifically, we describe a traveling wave of local field potential (LFP) activity in cortical area V4 of macaque monkeys that is triggered by the execution of saccadic eye movements. These waves sweep across the V4 retinotopic map, following a consistent path from the foveal to the peripheral representations of space; their amplitudes correlate with the direction and size of each saccade. Moreover, these waves are associated with a reorganization of the postsaccadic neuronal firing patterns, which follow a similar retinotopic progression, potentially prioritizing the processing of behaviorally relevant stimuli.

INTRODUCTION

Oscillations are a ubiquitous property of neural activity, as measured with intracranial electrodes or with EEG (Buzsaki, 2006; Buzsáki and Draguhn, 2004). When such activity is measured simultaneously at multiple sites, the oscillations are often observed to be synchronous, and this synchrony has been hypothesized to play a role in various functions, such as long-range communication and sensory perception (Singer and Gray, 1995; Sompolinsky et al., 1990; Varela et al., 2001).

Synchronous oscillations are usually observed to be coherent in space, meaning that the temporal progression of activity has identical phase across recording sites. However, out-of-phase synchronous oscillations also exist, and occasionally they give rise to complex spatiotemporal patterns of activity in the form of traveling waves (Wu et al., 2008). Such waves have been found in a variety of brain areas, including the hippocampus, olfactory bulb, motor cortex, auditory cortex, barrel cortex, and the visual cortex (Wu et al., 2008). Despite this frequent observation of traveling waves, their functional role remains unclear: traveling waves in sensory cortex do not generally encode sensory stimuli (Chen et al., 2006; Jancke et al., 2004; Xu et al., 2007), and waves in motor cortex do not encode movement parameters, although they have been implicated in the processing of movement-related information (Rubino et al., 2006; Takahashi et al., 2011).

Several studies have shown that oscillatory activity is coupled with modulations of single-neuron excitability (Jacobs et al., 2007; Jansen and Brandt, 1991; Lakatos et al., 2005) and spike timing (O'Keefe and Recce, 1993). This suggests that oscillations are predictive of the relative sensitivity of multiple neurons within a population: in-phase oscillations imply similar sensitivity at each point in time across the population, while out-of-phase oscillations reflect assignment of high sensitivity to different neuronal subpopulations at different times. The case of out-of-phase oscillations is particularly interesting, as it could relate to the prioritization of processing within specific subpopulations: one hypothesis is that traveling waves reflect a sequential change in neuronal processing, which would allow the brain to prioritize the processing of behaviorally relevant signals (Ermentrout and Kleinfeld, 2001).

In the primate visual system, behaviorally relevant stimuli are brought into view by saccades, which are rapid eye movements that center the object of interest on the high-resolution part of the retina. Saccades are made several times per second, and they are associated with transient periods of very low visual sensitivity (Ross et al., 2001). Consequently, the visual system must extract information rapidly and efficiently during the epochs between saccades, by integrating oculomotor and visual signals (Teichert et al., 2010). We therefore hypothesized that traveling waves might reflect the spatiotemporal reorganization of visual information processing across visual space, during the epochs between the completion of one saccade and the initiation of the next.

We tested this idea by recording neural activity, in the form of local field potentials (LFPs) and spiking responses, in cortical area V4 of macaque monkeys chronically implanted with multielectrode arrays. V4 neurons are selective for specific visual stimulus features, and each area V4 contains a retinotopic representation of the contralateral visual hemifield (Gattass et al., 1988; Mineault et al., 2013). We found that saccades triggered robust traveling waves of oscillatory LFP activity that consistently swept from the foveal to the peripheral zones of the V4 retinotopic map. Importantly, single-neuron sensitivity after saccades followed the same sequence, such that foveal neuron sensitivity increased shortly after a saccade, with peripheral neuron sensitivity peaking at longer time lags. Thus, we hypothesize that traveling waves reflect a functional mechanism of

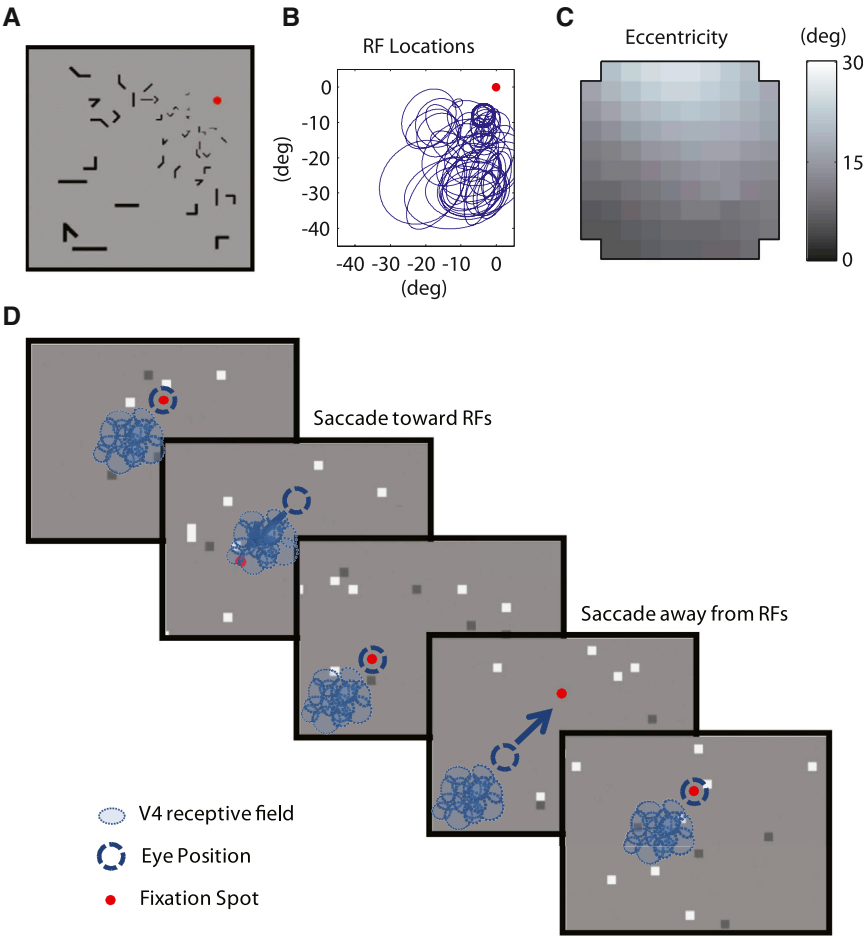

Figure 1. Receptive Field Mapping and Saccade Experiments

(A) Sample stimulus frame of the Receptive Field Mapping experiments. The stimulus was composed of sparse bars arranged in a log-polar grid to account for the magnification of the visual field with eccentricity.

(B) Receptive fields of V4 neurons (blue ovals), estimated with data recorded from one day of experiments in one monkey.

(C) Eccentricity (distance in degrees from fovea) of estimated LFP RFs, shown for all electrodes at their respective locations on the array.

(D) Schematic diagram of the saccade experiment. Monkeys made saccades (blue arrow) to visual targets (red dot) over a sparse white noise background stimulus, composed of dark gray and white dots against a light gray background. The receptive fields (RFs) of the neurons and the LFPs (blue ovals) captured from the microelectrode array were positioned in both monkeys in the lower left part of the visual field, thus separating the saccades into two groups, saccades toward and away from the RFs.

prioritizing the bottom-up processing of visual stimuli that are chosen, based on behavioral context, as the targets of saccades.

RESULTS

Occurrence of Traveling Waves in Cortical Area V4

The receptive fields (RFs) of V4 neurons and LFPs are organized retinotopically, so that V4 in each hemisphere contains a map of contralateral visual space (Gattass et al., 1988; Mineault et al., 2013). In order to study the dynamics of neural activity across this map, we implanted 10 × 10 electrode arrays (4 mm × 4mm) into dorsal V4 of two macaque monkeys. The arrays were placed so as to cover a sizeable portion of the parafoveal visual representation.

We computed the centers of LFP RFs, based on responses to a rapidly changing sequence of flashed bars (Figure 1A; Mineault et al., 2013). For the example shown in Figure 1B, the ensemble of RF centers computed from one recording covered roughly 27 degrees of visual angle, with retinal eccentricities ranging from 3 to 30 degrees. Notably, the gradient of retinal eccentricity on the array (Figure 1C) was quite smooth, with more foveal sites (darker gray) closer to the bottom of the array, and peripheral sites (lighter gray) closer to the top.

To study V4 activity during saccades, we used the paradigm shown in Figure 1D, in which monkeys made saccades toward and away from the area of visual space accessible to the arrays. These saccades were cued by the appearance of a visual target, as shown in Figure 1D. During the experiments, the saccade target stepped back and forth, at unpredictable intervals, so that monkeys made many (typically 3,000–4,000) saccades in each session; mean eye position traces for one session are shown in Figure 2A. Throughout performance of this task, we also probed visual responses with a sparse noise stimulus, which consisted of random white and black squares that changed position on each frame. We used this stimulus to evoke perisaccadic responses in V4 (described below) without introducing stimulus-induced response correlations in space or time.

To examine the spatiotemporal properties of V4 oscillations, we focused on LFP activity in the beta band (20–40 Hz); consistent with previous work (Henrie and Shapley, 2005), LFP power in this band was small (~1%) relative to that of the total spectral power of our recordings. This band was chosen based on previous results on traveling cortical waves (Rubino et al., 2006) and on our observation that spatial coherence was largest at these frequencies (Figure S1A). Spatial coherence is a signature of traveling waves, as it indicates a systematic relationship between the instantaneous phases of oscillations at different points in space.

To improve signal quality, the beta LFP was averaged across saccades within a single day of recording unless otherwise mentioned. Figure 2B shows this mean activity for six electrodes, taken from various times points around saccades (n = 1880) made toward the receptive fields detectable on the array. These

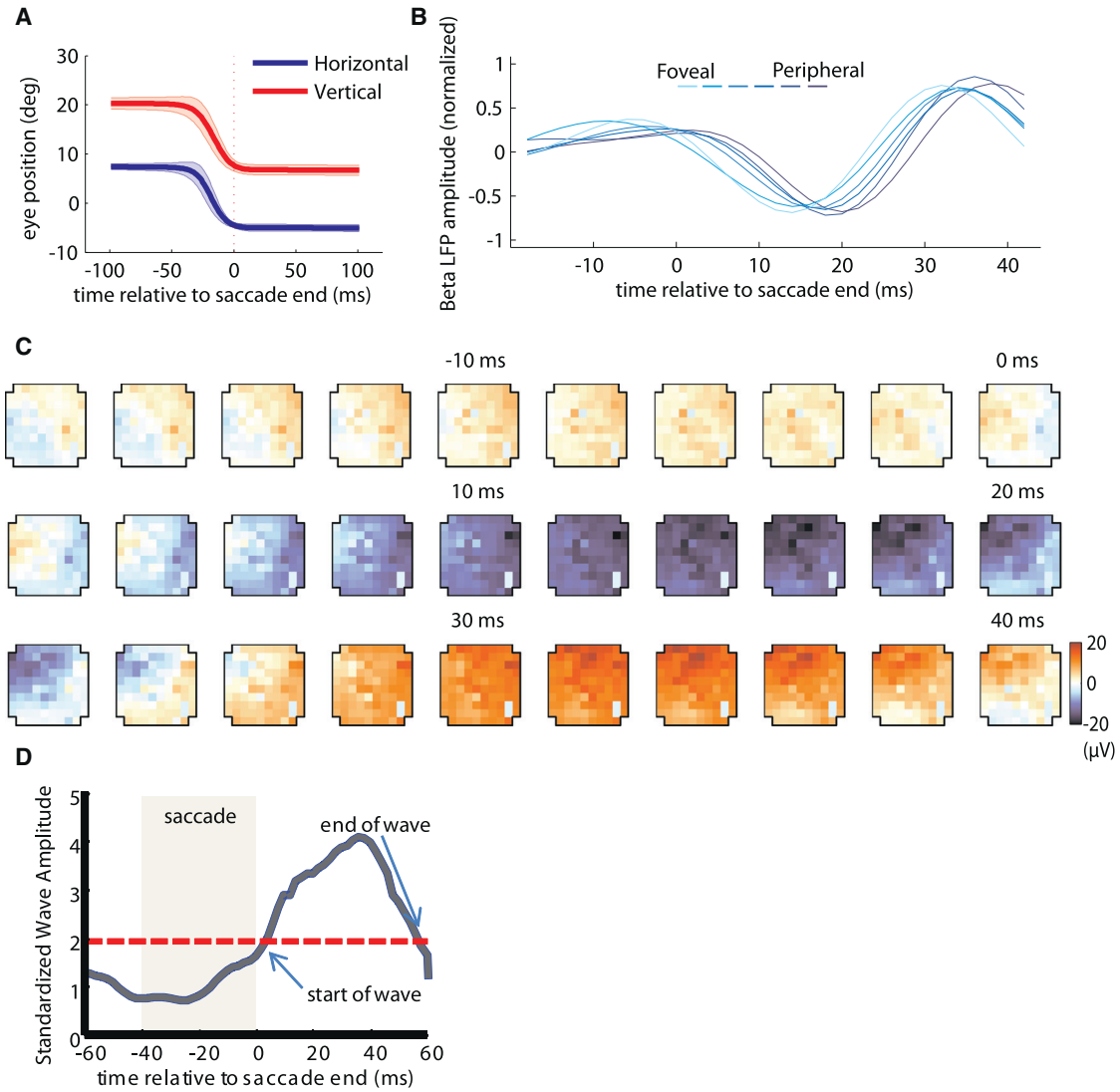

Figure 2. Occurrence of Traveling Waves in Area V4

(A) Average eye position traces for saccades directed toward the RFs accessible to the array, with horizontal (blue) and vertical (red) eye positions plotted. Time zero is defined as the end of the saccade.

(B) Normalized beta LFP amplitude around the time of saccade end, averaged across all saccade trials, for 6 electrodes (light blue for more foveal, starting at 3 degrees eccentricity; darker blue for more peripheral electrodes, up to 26 degrees eccentricity).

(C) Mean perisaccadic beta LFP activity at various time points relative to a saccade made toward the RFs, recorded on one array. Beta-band LFP amplitude is color coded, with red indicating positive amplitude and blue indicating negative amplitude.

(D) Temporal evolution of the amplitude of the wave is illustrated in (B) and (C). The red dotted line indicates the wave detection threshold, and the gray shading indicates the saccade.

electrodes were estimated to have receptive field eccentricities that spanned the range from low (light blue) to high (dark blue). Interestingly, the beta LFP oscillation for the more peripheral sites lags that for the foveal sites, suggesting the existence of out-of-phase oscillations that begin shortly after each saccade (time 0 on the x axis). Figure 2C shows the spatiotemporal evolution of the beta-band LFP around the time of the saccade, with each panel representing the mean activity for all electrodes at a single time point. Beta-band LFP amplitude is color coded, with red colors indicating large positive amplitudes, and blue colors indicating large negative amplitudes (mean beta amplitude is 20 μV).

Inspection of Figure 2C reveals a traveling wave that propagates from the lower right to the upper left of the array, beginning shortly after the termination of the saccade. The spatial extent of the wave is larger than that of the array, but a wave front is clearly visible between roughly 20 and 30 ms. We observed similar postsaccadic waves in both monkeys throughout many different days of recordings. We also observed patterned LFP activity that was triggered by spikes (Nauhaus et al., 2009) and in other

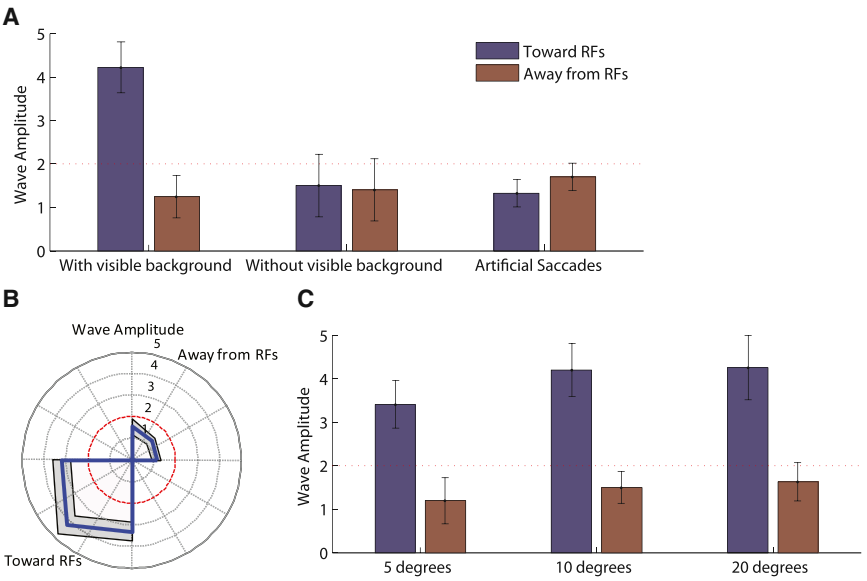

Figure 3. Properties of Traveling Waves in V4

Mean standardized (z-scored) amplitude values derived from the wave algorithm for (**A**) experiments for the standard saccade paradigm (left), saccades performed in the absence of any visible background (center), and artificial saccades (right).

(B) Mean wave amplitude for experiments with different saccade directions. Black lines indicate standard error of the mean.

(C) Wave amplitudes for experiments of different saccade sizes. Red dashed line indicates the wave detection threshold (2).

frequency bands, but we focus here on the beta-band LFP waves, which in our study showed the clearest spatiotemporal relationship to the saccades (Figure S1A).

Traveling Waves in V4 Require Both Oculomotor and Visual Activity

To characterize traveling waves in an objective and quantitative manner, we employed a wave detection algorithm, which fit the parameters of a two-dimensional wave equation to data of the kind shown in Figure 2C. In this approach, LFP activity across each array was characterized as a pure sinusoidal space-time wave (see Experimental Procedures), which included parameters corresponding to the speed, direction, and amplitude of each wave. This model generally provided a very good fit to the data (median R^2 0.70); an example fit for the data in Figure 2B is shown in Figure S1C.

Of the model parameters, the amplitude is particularly important, as it allows us to detect the occurrence of the wave: Unstructured oscillatory activity would correspond to wave amplitudes near zero (Figure S2). We therefore considered a wave to have occurred when the amplitude parameter recovered by the algorithm exceeded two standard deviations above the mean baseline value calculated during periods of steady fixation. Figure 2D shows the temporal evolution of the amplitude of the wave illustrated in Figures 2B and 2C.

We examined wave amplitudes for *toward* saccades (those directed toward the RFs accessible to the array) and *away* saccades (those directed in the opposite direction). For toward saccades, we observed similar wave activity in a large majority of recording sessions (16/17 sessions for monkey #1 and 23/25 sessions for monkey #2). The mean wave amplitude for these sessions was significantly above threshold (Wilcoxon right-tailed test, $p < 0.01$), with the average time of occurrence being 8.8 ms (± 7.2 ms) relative to the saccade end. Average wave duration was 37.7 ms (± 8.6 ms). Thus traveling waves occurred shortly after saccades directed toward the LFP RFs and lasted for roughly one cycle of the beta oscillation. As detailed below, these waves were typically followed by synchronized firing of individual neurons.

Significant wave activity was detected at a much lower rate with away saccades (9/42 sessions), and the mean wave amplitudes for these saccades were significantly below threshold (Wilcoxon left-tailed test, $p < 0.01$; see Figure S2 for an example and Figure 3A for amplitude averages across sessions). Moreover, the properties of this wave activity were not consistent from session to session, as shown below.

To ensure that these results were not due to averaging of LFP data across trials, we applied the same methods to estimate wave activity on individual trials. Significant waves were present on 67.3% (37,472 out of 55,647) of toward saccade trials. For saccades away from the RFs, waves were present in 20.6% (8,283 out of 40,155) of the trials. The average amplitude histograms of all waves detected is plotted in Figure S5B.

In control experiments we found that traveling LFP waves in V4 required visual stimulation, as they did not generally occur when the same experiments were conducted in the absence of any visible background for either saccade direction (Figure 3A; Wilcoxon left-tailed test against the detection threshold, $p < 0.01$). Importantly, this result also controls for the possibility that the waves were triggered by the appearance or disappearance of the saccade target. Thus the waves required background visual stimulation, although the precise temporal structure of the stimulation was not important: Saccades made over static backgrounds (7 experiments: 3 in monkey #1 and 4 in monkey #2) generated waves of similar strength to those found with spatiotemporally random backgrounds (Figures S3C and S3D).

This latter result raises the possibility that the waves were due entirely to changes in retinal stimulation during the saccade, rather than to the execution of the saccade per se. We tested this possibility by measuring V4 responses to artificial saccades, in which the background stimulus (Figure 1D) was swept across the visual field at saccadic velocities, while the monkeys maintained fixation. This condition did not lead to the appearance of traveling waves for either saccade direction (Figure 3A, Wilcoxon left-tailed test against the detection threshold, $p < 0.01$). In additional control experiments we found that traveling waves did not depend on eye position before or after the saccade

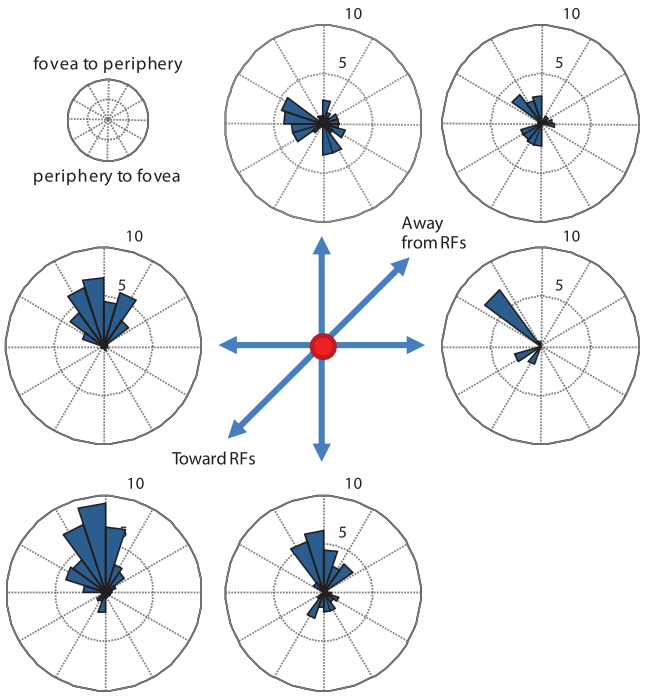

Figure 4. Traveling Waves Propagate along the V4 Retinotopic Map
Retinotopic wave directions for six saccade directions (toward, toward + 45°, toward − 45°, away, away + 45°, away − 45°). Histograms of the wave directions for each postsaccadic traveling wave. Angle values were rotated for both monkeys so that upward angles correspond to a foveofugal direction (as determined by the retinal eccentricity gradient).

(Figures S3B and S3D; Wilcoxon test, $p = 0.6108$ for amplitude and circular one sample test, $p = 0.43$ for direction) or on the predictability of the impending saccade target location (Figure S3D, Wilcoxon test, $p = 0.8912$).

Traveling Waves in V4 Correlate with Saccade Direction and Size

To obtain a more detailed picture of the relationship between wave amplitude and saccade direction, we performed additional experiments in which the saccade vector was rotated 45 degrees clockwise or counter-clockwise from the ensemble of receptive field centers. These conditions still evoked traveling waves, but the mean amplitude decreased (Wilcoxon tests, both $p < 0.01$; Figure 3B), revealing a significant tuning of the wave amplitude for saccade direction (Rayleigh test, $p < 0.001$). There was also a significant relationship between saccade size and wave amplitude (linear regression, $\beta = 0.143$, $\varepsilon = 2.59$, $n = 42$, $p < 0.001$; Figure 3C), though there was little modulation of amplitude for saccades greater than 10 degrees (t test, $p = 0.34$), showing a saturation of the wave amplitude for larger saccade sizes.

Traveling Waves Propagate along the V4 Retinotopic Map

While the amplitude of the traveling wave was modulated by the saccade direction and size, we found that the *direction* of the traveling wave on the cortical surface was largely invariant to the properties of the eye movements. In general, as is apparent from the examples shown in Figures 2C and S3C, the waves tended to propagate from low- to high-eccentricity visual locations. To examine this trend across experimental conditions, we compared the dominant wave direction for all experiments involving toward saccades ($n = 20$) to the eccentricity gradient estimated from retinotopic maps of the kind shown in Figure 1C.

Figure 4 shows histograms of the retinotopic direction of the postsaccadic waves, for six saccade directions (toward, toward + 45°, toward − 45°, away, away + 45°, away − 45°). Across sessions, traveling waves maintained a consistent retinotopic direction, propagating from more foveal to more peripheral electrodes on the array, for all three saccade directions within 45° of the ensemble of V4 RFs. The direction of the wave was not significantly different from that of the eccentricity gradient (average deviations 13.2 degrees in monkey #1 (circular one-sample test, $p = 0.26$, $n = 16$) and 5.7 degrees in monkey #2 ($p = 0.53$, $n = 23$).

Figure S3A shows that the consistency of the postsaccadic wave direction holds for different saccade sizes as well. In contrast, the few waves that occurred following saccades away from the V4 RFs did not exhibit a consistent retinotopic direction preference. Similar results were observed for waves detected on individual trials: propagation was from foveal to peripheral zones after toward saccades, with no consistent direction being apparent for away saccades (Figure S5C).

In addition to the direction of propagation, we also recovered the speed of propagation for each traveling wave from the fits to the wave equation. This quantity provides some insight into the potential anatomical substrate underlying the waves, as the speed of propagation of neural signals along lateral connections is limited by the biophysical properties of unmyelinated cortical axons. Previous work has estimated this speed as roughly 30 cm/s (Gilbert and Wiesel, 1983). For V4 waves, the propagation speed was quite consistent, following a normal distribution around a mean of 31 cm/s and a standard deviation of 8 cm/s. The wavelength also followed a normal distribution with a mean value of 1.21 cm and a standard deviation of 0.23 cm. Thus, although it is difficult to infer the relevant anatomical substrate from neural activity (Sit et al., 2009), our results are consistent with the suggestion that traveling cortical waves propagate along lateral connections (Ermentrout and Kleinfeld, 2001; Nauhaus et al., 2009; Rubino et al., 2006; Takahashi et al., 2011; Xu et al., 2007).

To summarize, postsaccadic LFP traveling waves sweep from foveal to peripheral zones of contralateral V4 at a constant speed in cortical space; they are stronger for saccade directions toward the RFs; they are independent of eye position, target predictability, and structure of the visual background; and they do not occur after simulated saccades or saccades in the dark. These waves are robust phenomena that can readily be observed on individual trials.

Traveling Waves Are Associated with Changes in Neuronal Excitability

Having established the existence of postsaccadic traveling waves in V4, we next examined single-neuron excitability in the periods between eye movements. Many previous studies

have documented a relationship between neuronal firing and the properties of ongoing oscillations that are detectable in the LFPs (Engel et al., 1991; Pesaran et al., 2002; Womelsdorf et al., 2007). We therefore examined the relationship between saccades and LFP phase, as well as the relationship between LFP phase and single-neuron firing.

Relationship between Saccades and LFP Phase

In our data, saccades typically had little influence on the amplitude of the beta oscillation (Figure S1B), suggesting that the modulation of the LFP seen in the previous sections was due to a pure phase reset (Bartlett et al., 2011; Ito et al., 2011; Rajkai et al., 2008). Figure 5A provides evidence for phase resetting of the beta LFP signal recorded on one electrode from the array, for the example wave shown in Figure 2. The two histograms show the distribution of beta LFP phases, across all saccade trials, 5 ms before (left) and 5 ms after (right) the end of the saccade. The beta LFP phase distribution follows a uniform distribution before the end of the saccade (Rayleigh test, $p = 0.7138$) but deviates significantly from uniformity after the end of the saccade (Rayleigh test, $p < 0.001$), indicating significant phase tuning. Thus the phase of the beta LFP oscillation was reset to a specific value (near -0.5 radians) at a time very close to the end of the saccade.

Figure 5B shows the progression of this phase resetting across all the electrodes of the array at different times relative to the end of the saccade. The colors denote sites that had significant beta phase tuning (see Experimental Procedures for definition) at each time point following a saccade; black indicates a lack of significant tuning. As indicated in the figure, the phase resetting is first seen near the foveal representation (lower right on the array) of visual space, and this resetting occurs near the end of the saccade (time = 0 ms). As time progresses, the phases are reset at more peripheral locations, while the more foveal locations advance to other phase values. Thus, for this example, the postsaccadic traveling wave entails a progression of the reset phase from relatively foveal to relatively peripheral locations on the V4 retinotopic map.

To examine the consistency of this finding across days of recordings, we plotted the reset phases as a function of location on the retinotopic map. Figure 5C shows this result for four different time points: -5, 0, 5, and 10 ms relative to the end of the saccade toward the RFs. Here each dot corresponds to the reset phase for each electrode across 20 different experiments, and the colors indicate the sites that became tuned at the corresponding time points. For example, sites that exhibited significant phase resetting immediately at postsaccadic time zero (Figure 6C, upper right) are colored red, and it is clear that these sites tend to be close to the foveal representation. Sites that first exhibit significant tuning at 10 ms after the saccade (blue dots, Figure 6C, lower right) tend to have more peripheral receptive fields; however the postsaccadic phase is again close to the phase to which foveal sites are reset right after saccade end.

Relationship between LFP Phase and Neuronal Firing

Given that the beta phase was locked to saccade offset (Figure 5), we next sought to determine whether spiking in V4 was locked to the beta phase. To separate spike-LFP relationships from saccade influences, we analyzed data obtained during the RF mapping procedure, which required fixation. If the beta LFP were uncorrelated with spiking activity, then spikes would occur with equal frequency at all phases of the beta oscillation. In contrast, we found that the vast majority of visually responsive neurons exhibited significant phase tuning (631/657, Rayleigh test, $p < 0.001$). Moreover the tuning was highly consistent from neuron to neuron, with most neurons exhibiting a *preferred phase* (Jacobs et al., 2007) near -2.85 radians (Figure 6A). This preference was independent of receptive field eccentricity (linear regression, $r = -0.07$, $p = 0.45$).

The clear phase preference exhibited by most V4 neurons suggests that the phase reset shown in Figure 5 could influence the timing of postsaccadic spikes in single neurons. To test this idea, we analyzed data from 180 neurons recorded during experiments ($n = 10$) in which at least 1,500 total saccades were completed. Because visual stimulation due to the sparse noise stimulus was, on average, identical across time and saccade direction, any changes in the spiking responses were related to the execution of the saccades.

Saccades dramatically reorganized the timing of single-neuron responses in V4. Figure 7 shows a histogram of single-neuron response latencies following toward (Figure 7A) and away (Figure 7B) saccades. For away saccades, latencies ranged from 40 to 140 ms, with a unimodal peak near 75 ms, similar to what has been reported previously (Lee et al., 2007; Sundberg et al., 2012). A similar distribution of latencies was found during fixation, in the RF mapping experiments (Figure 7C; two sample t test $p = 0.723$). In contrast, latencies following toward saccades were bimodally distributed (Hartigan's Dip test, $p < 0.005$), with one mode at 61 ms and a second mode at 119.5 ms (Gaussian mixture distribution with two components). These two modes were separated by 58.5 ms, which was roughly one cycle of the dominant frequency in the beta band plus the $\sim$15ms delay of phase resetting between the foveal and peripheral zones in V4 (Figure 5B).

The first mode in the latency distribution was close to the minimum visual latency in V4, as shown in our fixation data and reported previously by others (Lee et al., 2007; Sundberg et al., 2012). Interestingly, neurons from the short-latency group for toward saccades tended to have receptive fields with small eccentricities (mean eccentricity of 6.7 degrees) compared to those in the long-latency group (mean eccentricity of 13.5 degrees). For both groups, the timing of firing was tightly linked to the underlying beta oscillation: Neurons fired when the instantaneous phase was near the preferred phase (Figures 6B, left and 6C, right), after which the oscillation became desynchronized (Figure 6C, left). More specifically, for the time window around the first mode (61 ms, Figure 6B), foveal sites (left panel) had mean phase values that did not differ significantly from the preferred phase (circular one sample test, $p = 0.11$) while peripheral sites (right panel) had values far from this value and close to the anti-preferred phase. For the time window around the second mode (119.5 ms, Figure 6C), foveal sites exhibit a uniform distribution (Rayleigh test, $p = 0.28$), while the peripheral sites retained their tuning and had values that did not differ significantly from the preferred phase (circular one-sample test, $p = 0.21$).

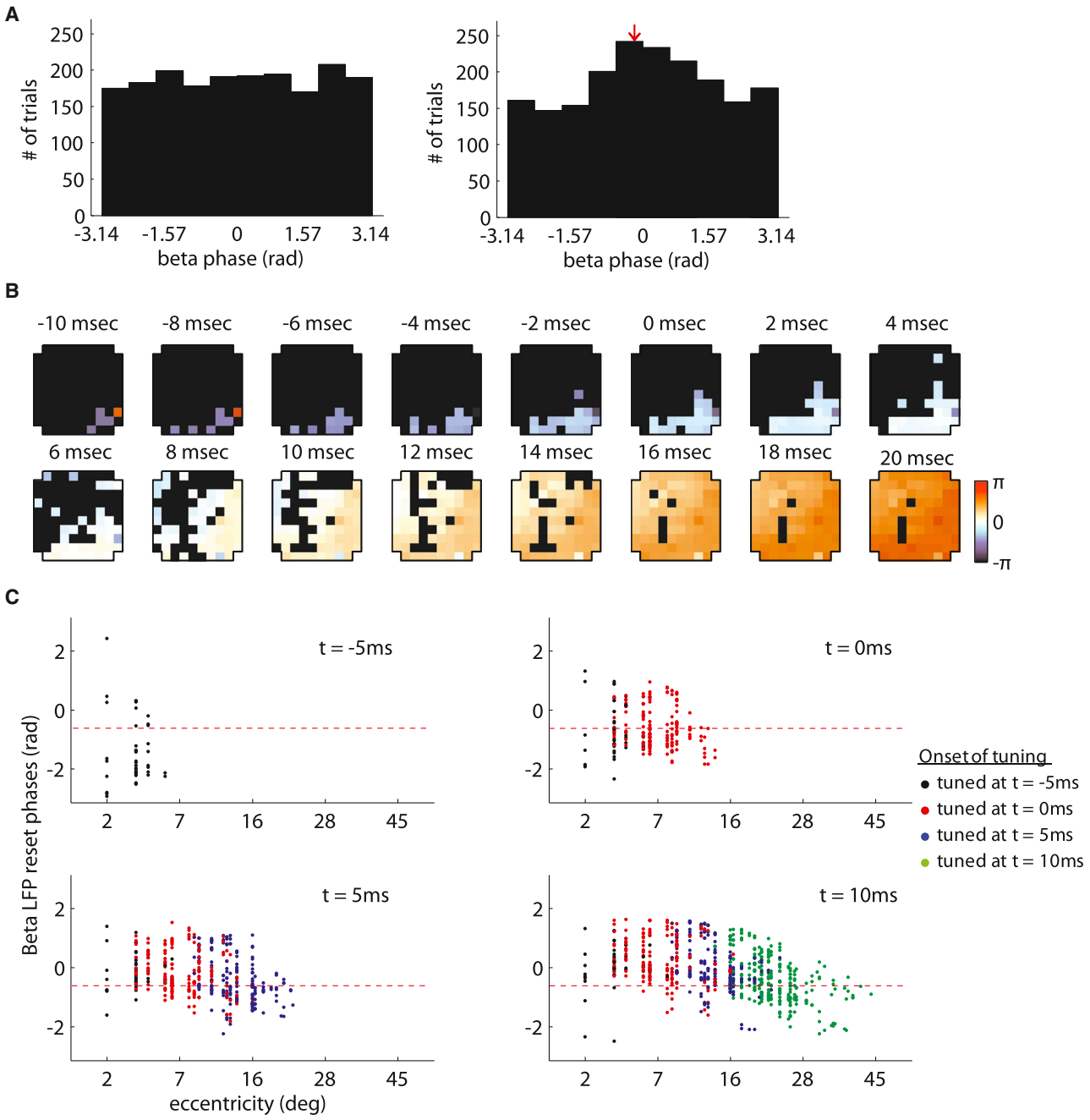

Figure 5. Traveling Waves Reflect a Sequential Resetting of Beta LFP Phase

(A) Phase resetting of the beta LFP signal recorded on one electrode, for the example wave shown in Figure 2. The two histograms show the distributions of beta LFP phases, across all saccade trials (n = 1880), 5 ms before (left) and 5 ms after (right) the end of a saccade toward the RFs.

(B) Progression of phase resetting across all the electrodes of the array at different times relative to the end of the saccade. The colors denote sites that had significant beta phase tuning, and the color corresponds to reset phase value; black indicates a lack of significant tuning.

(C) Reset phase as a function of location on the retinotopic map, across days of recordings, for four different time points: −5, 0, 5, and 10 ms relative to the end of saccades toward the RFs. Each point represents one electrode on one recording day at the time that its beta phase was reset. The y value corresponds to the circular mean reset phase. The points shown in each panel represent all tuned electrodes across 20 different experiments, and the colors indicate the sites that became tuned at these four different time points.

For the population as a whole, there was a significant correlation between receptive field eccentricity and response latency following toward saccades (Spearman $r = 0.45$, $p < 0.005$), but not for away saccades (Spearman $r = 0.01$, $p = 0.96$) or during fixation (Spearman $r = -0.05$, $p = 0.51$). Overall these results suggest that postsaccadic traveling waves were associated

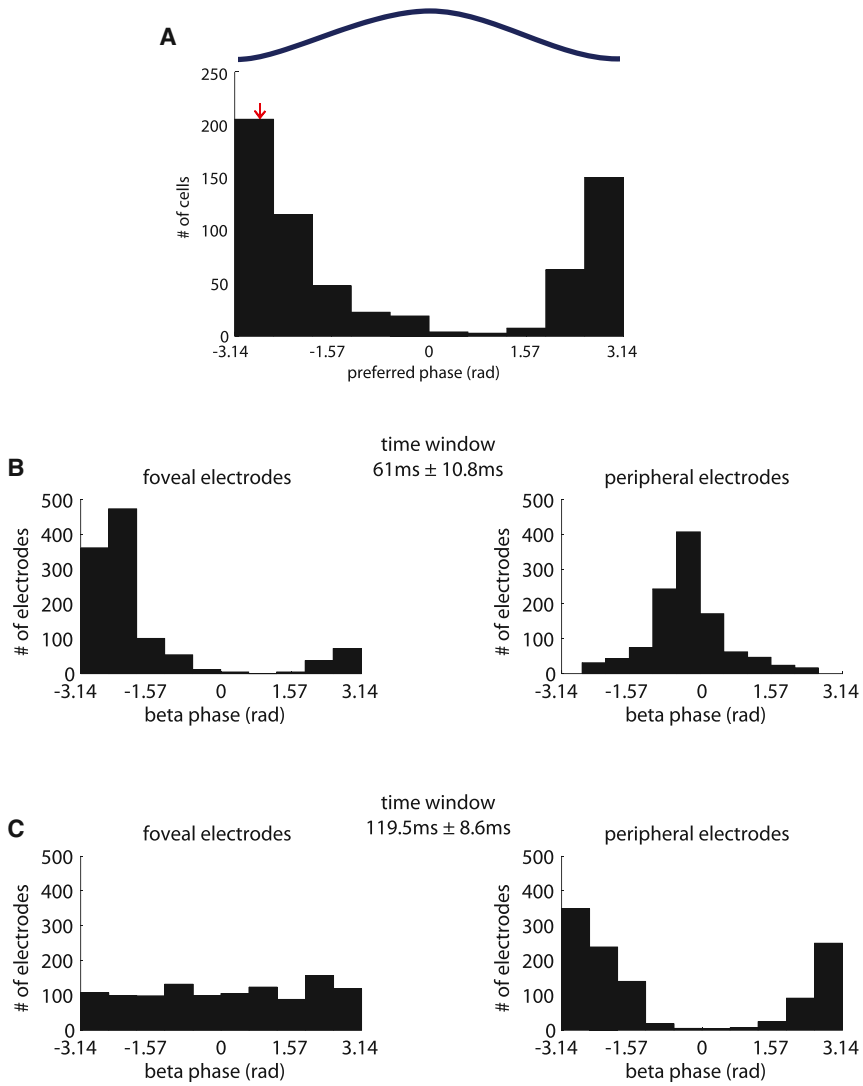

Figure 6. Preferred Phases of V4 Neurons

(A) Histogram of preferred phases for the V4 neurons that exhibited significant phase tuning (n = 631). The red arrow indicates the circular mean of the preferred phase distributions (−2.85 radians).

(B) Instantaneous phases across 20 different saccade experiments (a total of 1,120 values), calculated around the earlier mode of the neuronal latency distribution shown in Figure 7A (time window of 61 ms ± 10.8 ms after the onset of fixation). Left panel shows the distribution of circular mean phase values for all foveal (< 10 degrees eccentricity, 56 in total, 20 for monkey #1 and 36 for monkey #2); right panel shows the same for peripheral electrodes (> 10 degrees eccentricity, 56 in total, 17 for monkey #1 and 39 for monkey #2).

(C) Same distributions as the previous panel, around the mode of the second mode of the neuronal latency distribution of Figure 7A (time window 119.5 ± 8.6 ms after the onset of fixation).

with a qualitatively similar spatiotemporal progression of single-neuron firing (Figure S4B), with the sequence of postsaccadic responses being linked to RF eccentricity.

In summary, we find that each saccade resets the phase of the beta oscillation for recording sites with receptive fields near the fovea. The same phase reset occurs some time later for oscillations at more peripheral sites. Following this reset, neurons are most likely to fire when the beta oscillation reaches their preferred phase; this firing is delayed by one cycle for peripheral recording sites relative to more foveal ones.

DISCUSSION

We have shown that saccadic eye movements made in the presence of visual stimulation trigger traveling waves of oscillatory LFP activity in cortical area V4. The waves propagate from foveal to peripheral parts of the retinotopic map and qualitatively predict the timing of single-neuron firing. Traveling waves thus reflect a mechanism by which the oculomotor system might exert control over the spatiotemporal organization of sensory processing.

Comparison to Previous Work

Our findings are consistent with previous observations that saccades predictively reset the phase of ongoing oscillations in area V1, with concomitant effects on visual sensitivity (Rajkai et al., 2008) and spike-LFP synchronization (Bartlett et al., 2011; Ito et al., 2011). Such a phase reset is an abrupt change in the instantaneous phase of a signal comprised of multiple frequencies; it can result from small changes in the amplitudes of the oscillations comprising this signal.

Previous results focused on neural activity representing input from a small region of visual space, so that the spatiotemporal pattern of phase resetting was unknown. The nature of the phase resetting signal is of general importance, given the widespread observation that oscillatory phase correlates with neuronal sensitivity (Nikolić et al., 2013). In principle, phase resetting could occur synchronously at every point on the retinotopic map, in which case the visual system would alternate between periods of global sensitivity and insensitivity following each saccade (Ermentrout and Kleinfeld, 2001). In contrast, we have shown that phase resetting occurs sequentially across retinotopic space (Figure 5). Given the spatial extent of the wave (Figure 2) at any point in time, this should lead both to greater single-neuron visual sensitivity (Figure S4B) and greater synchrony among neurons (Ito et al., 2011) across roughly 2 mm of cortex. In visual space, this distance translates to 5–8 degrees of eccentricity for the parafovea and 15–20 for more peripheral areas.

Our results are relevant to the hypothesis that oscillations provide a means of facilitating interactions between the visual and

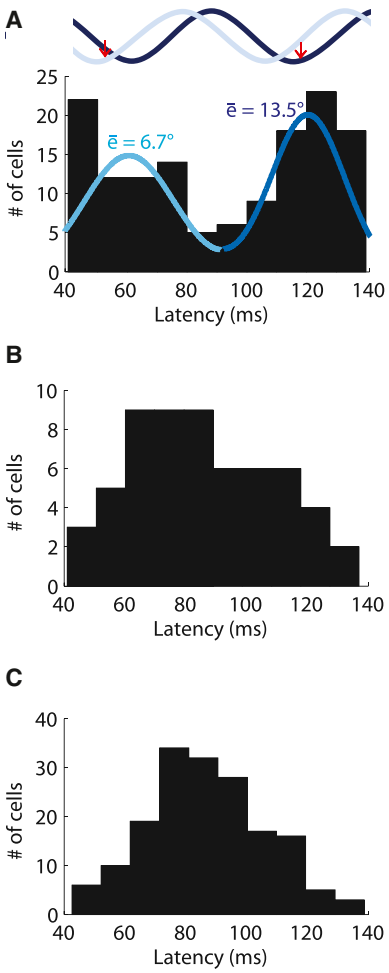

Figure 7. Saccades Reorganize the Timing of Single-Neuron Responses in Area V4

(A) Histogram of postsaccadic response latencies for saccades toward the RFs. Superimposed on the histogram is the mixture of two Gaussian distributions fitted to the histogram, with one mode at 61 ms and a second mode at 119.5 ms. These two distributions contain neurons of different eccentricities, mainly foveal neurons for the first distribution (mean eccentricity of 6.7 degrees) and more peripheral for the second distribution (mean eccentricity of 13.5 degrees). The timing of firing of the two groups was tightly linked to the occurrence of the preferred phase (red arrows on the inset above the histogram) for foveal (light blue) and peripheral (dark blue) beta LFPs.

(B) Histogram of postsaccadic response latencies for saccades away from the RFs.

(**C**) Histogram of receptive field response latencies during steady fixation.

oculomotor modalities. Previous work has shown that oscillatory phase resetting allows for interactions between somatosensory and auditory processing (Lakatos et al., 2007) and between auditory and visual processing (Kayser et al., 2008; Lakatos et al., 2009).They also allow for interactions between motor and sensory processing (Bartlett et al., 2011; Rajkai et al., 2008), with neuronal effects being evident even in primary sensory areas. To our knowledge these previous experiments have not examined the spatial pattern of phase resetting; it would be interesting to determine whether the cross-modal oscillatory effects observed in other systems follow a spatial pattern similar to that reported here.

Numerous studies have shown that traveling waves in sensory brain regions occur with the appearance of a stimulus, although there is generally no reported relationship between the identity of the stimulus and the structure of the waves (Xu et al., 2007). In visual cortex, these waves bear a certain similarity to those reported here, since they propagate retinotopically along lateral connections (Benucci et al., 2007; Gao et al., 2012; Nauhaus et al., 2009). However, we suspect that these waves represent a different phenomenon, as some of them are strongest in the absence of visual stimuli, whereas the V4 waves reported here require visual stimulation (Figure 4C). Moreover, the amplitude of waves reported in V1 typically decreases with distance from the point of origin (Nauhaus et al., 2009), whereas the postsaccadic waves in V4 maintain a similar amplitude across retinotopic positions (Figure 2). Finally, waves in V4 precede changes in spiking activity (Figure 7), whereas V1 waves appear to be active and caused by synaptic interactions (Gao et al., 2012) and often triggered by spikes (Nauhaus et al., 2009; but see Ray and Maunsell, 2011 for a different interpretation).

In motor cortex, traveling waves are often associated with reaching movements in human (Takahashi et al., 2011) and non-human (Rubino et al., 2006) primates. These waves are similar to the ones reported here in that they are carried by the beta-band LFP and follow known anatomical connections. Interestingly, motor cortex waves also appear to be cross-modal in nature, as they encode the location of visual cues, rather than the parameters of the corresponding motor actions (Rubino et al., 2006). The idea that oscillations could reflect differential processing in specific neuronal subpopulations has found support in various cortical areas and for various LFP frequencies (Destexhe et al., 1999; Fries et al., 2008; Jacobs et al., 2007; Pesaran et al., 2002; Zanos et al., 2012), particularly those around 20 Hz (Engel et al., 1991; Pesaran et al., 2002; Womelsdorf et al., 2007). In most studies, this relationship is characterized by a phase preference of the kind described above (Figure 6).

Theoretical Importance

The properties of oscillatory activity are often modeled mathematically via a network of coupled oscillators, which naturally give rise to wave-like patterns (Ermentrout and Kleinfeld, 2001; Heitmann et al., 2012). One particularly relevant model (Heitmann et al., 2012) demonstrates that beta oscillations with random phases can be organized into a specific wave pattern by transient signals that modulate the strength of inhibitory connectivity across the network. Thus the saccadic suppression that occurs in V4 (Kleiser et al., 2004) may result from transient activation of local inhibitory V4 circuits; this activation could then initiate the transition to a wave pattern at the end of the saccade (Heitmann et al., 2012). Previous work has suggested that the timing of oculomotor activity in the superior colliculus is consistent with a role in triggering saccadic suppression (Churan et al., 2012).

Relationship to Perception and Behavior

Humans and other primates make thousands of saccades each day, and there is ample evidence that the brain combines

oculomotor and visual signals to optimize perception around the time that the eye is moving (Teichert et al., 2010). Saccadic suppression is one well-studied example of such visuomotor integration: each saccade triggers a decrease in contrast sensitivity, which begins before saccade onset and is often followed by an increase in sensitivity (post-saccadic enhancement) after the completion of the saccade (Knöll et al., 2011).

Objects are typically selected as the targets of saccades because they have some potential behavioral relevance (i.e., an approaching predator, etc.). However, the act of foveating a target does not guarantee that it will be processed more rapidly or attentively by the rest of the brain. Irrelevant objects in the periphery can, for example, have greater bottom-up salience (e.g., higher contrast). From Figure 7 of our paper, one can estimate that the traveling wave decreases latencies at low-eccentricity locations by 10−30 ms; this is equivalent to the latency decrease found with an increase in contrast on the order of 50%–80% (Sundberg et al., 2012). Thus foveal stimuli become more salient for the visual system during the immediate postsaccadic interval, and this effect resembles post-saccadic enhancement. However, psychophysical studies have not generally found that post-saccadic enhancement is spatially or temporally specific (Knöll et al., 2011), as would be predicted from our results. Moreover, post-saccadic enhancement appears to occur primarily for chromatic stimuli (Knöll et al., 2011), which we have not examined here. Thus, a more likely psychophysical correlate of the traveling wave is a recovery from saccadic suppression, which appears to occur earlier for foveal stimuli than for peripheral stimuli (Mitrani et al., 1970).

Saccades have previously been linked to traveling waves (albeit with different properties) in the superior colliculus (Munoz et al., 1991), suggesting that they may play a role in oculomotor control. In this regard V4 traveling waves may be linked to observations on humans free viewing natural stimuli (Wilming et al., 2013). These studies have revealed a phenomenon called saccadic momentum, in which individual saccades within a sequence are faster when they have the same direction as the previous saccade (Smith and Henderson, 2011). Because V4 traveling waves correlate with the shortening of latencies of visual responses in the region of visual space that contained the previous saccade target (Figure 7), they may contribute to saccadic momentum. The finding that saccadic momentum increases the probability of targeting previously unexplored parts of the visual scene (Wilming et al., 2013) thus suggests that traveling waves might be an important contributor to optimal sampling of space during natural vision.

EXPERIMENTAL PROCEDURES

Electrophysiological Recordings

The recording methods have been described previously (Mineault et al., 2013; Zanos et al., 2011a). Briefly, two macaque monkeys (*Macaca mulatta*) underwent a sterile surgical procedure for implantation of a headpost and a chronic 10 × 10 microelectrode array in area V4 (Utah array; Blackrock Microsystems). Area V4 was identified based on stereotactic coordinates, anatomical landmarks (Ghose and Ts'O, 1997) and the physiological properties of the neurons (Gattass et al., 1988). After recovery, each monkey was seated in a primate chair (Crist Instruments) and trained to maintain fixation and to make visually guided saccades toward stimuli presented on a screen, for liquid reward. All aspects of the experiments were approved by the Animal Care Committee of the Montreal Neurological Institute and were conducted in compliance with regulations established by the Canadian Council of Animal Care.

Signal acquisition and pre-processing.

We recorded wideband signals using a standard data acquisition system (Plexon Multichannel Acquisition Processor System), custom modified to allow sampling at 10 kHz (band-pass filtered using hardware filters between 0.07 and 2,500 Hz) over the 96 channels of each Utah array. Subsequent spike sorting and LFP analysis were performed through off-line digital filtering. We monitored the power spectrum of these wideband signals on a daily basis to minimize line noise and other artifacts. The remaining 60 Hz noise (and possible harmonics) were removed offline with a power spectrum correction method introduced previously (Zanos et al., 2011b). Recordings were referenced against a ground located on the skull 2–3 cm away from the array.

Offline-analysis was aimed at detecting single-neuron and LFP activity on each channel. To detect single-unit waveforms, we first band-pass filtered the raw signal between 500 and 4,000 Hz; spike detection and sorting were then performed using established methods (Quiroga et al., 2004). To avoid double-counting of single neurons during consecutive days of recordings, we began each recording session by displaying the same sequence of 100 natural images, repeated 10 times, while the monkey maintained fixation. The response of each neuron to this sequence, along with the shape of the action potential and the interspike interval histograms, were collected. We then computed pairwise correlations of these measures for all neurons found on different electrodes or days of recordings. Neurons that showed high correlations were deemed to be repeats and were discarded from further analysis.

We estimated the LFP signals by removing action potential waveforms from the wideband signal using a Bayesian method (Zanos et al., 2011b); the despiked signal was then band-pass filtered (0.2 to 150 Hz) and downsampled to 500 Hz to produce the LFP signals. All off-line digital filtering was implemented with Matlab software (Mathworks), using a fourth-order two-pass Butterworth filter (digital filter with zero phase delay).

Behavioral Task and Visual Stimuli

The visual stimuli were back-projected on a semi-transparent screen by a CRT video projector, refreshed at 75 Hz. The screen covered an area of 80 × 50 degrees of visual angle at a viewing distance of 78 cm. The monkeys were required to keep fixation within 1.5 degrees of the fixation point or saccade target for 500 ms to obtain a liquid reward on each trial. Eye position was monitored at 1,000 Hz using an infrared eye tracker (Eyelink; SR Research).

Receptive Field Mapping

To characterize visual receptive fields, we used a mapping procedure described previously (Mineault et al., 2013). The stimulus on each frame consisted of a gray background (7.0 cd/ m^2) and several (on average, 7) conjunctions of 2 black (< 2.0 cd/m^2) bars (forming angles of 45, 90, 135, or 180 degrees) positioned randomly and updated asynchronously, with each bar stimulus being displayed for 80 ms. The bar stimuli were placed along a 12 × 12 polar grid, such that stimuli at the periphery were longer and wider than those near the fovea; bar width was set to 0.25 times the eccentricity and the length of the bars was chosen so that no bars touched when presented simultaneously. Four different orientations were interleaved randomly. Stimulus positions were confined to the lower right corner of the screen (5–40 degrees of eccentricity for monkey #1 and 3–45 degrees of eccentricity for monkey #2) in order to maximally activate the neurons accessible to the arrays. The total extent of stimulation thus spanned 120° of polar angle. Bars appeared on screen for six stimulus frames (12.5 Hz; 80 ms) and the screen was refreshed at a rate of 75 Hz.

LFP and single-unit receptive fields were estimated using our previously published method (Mineault et al., 2013). Briefly, we found that multi-unit neuronal receptive fields were generally matched in preferred spatial position. However, because the LFP is the more robust signal, being present on nearly every electrode on every day of recording, we used the LFP to estimate retinotopy in the current paper. The retinotopic component of each LFP RF was well-captured by a Gaussian in log-polar coordinates (i.e., log-eccentricity and polar angle), while the gain of this envelope was modulated as a function of time lag (Mineault et al., 2013). We fit measured LFP responses through least-squares minimization of the parameters of the Gaussian function. A receptive field was deemed

significantly tuned if the fit to the Gaussian was significant at the $p < 0.0001$ level according to a $\chi 2$ test (Mineault et al., 2013; Wood, 2006).We then generated retinotopic maps of the kind shown in Figure 1C from the estimated values of the eccentricity at each electrode position. From these maps, retinotopic gradients were estimated (from foveal to more peripheral electrodes) as the average of the retinotopy difference between adjacent electrodes.

Saccade Experiments

As described previously in detail (Churan et al., 2011), for the saccade experiments, we used a random sparse noise stimulus to stimulate visual neurons in V4, without introducing stimulus related correlations in their activity. The sparse noise stimulus consisted of 50% black (< 2.0 cd/m^2) and 50% white (30.5 cd/m^2) squares (1 × 1 visual degrees) presented at random positions on a gray background (7.0 cd/m^2) (Figure 1A). The positions of the black and white squares changed randomly at the frame rate of 75 Hz; each square was 1 degree across, and collectively the squares covered 2% of the screen area on each frame. The amplitude and orientation of the visually guided saccades in each recording were constant, but they varied across recordings as described below.

At the beginning of each trial, there was a random 600 to 1400 ms fixation period before the saccade target was presented and the fixation point disappeared (Figure 1A). The monkey was then required to make a visually guided saccade to the target immediately after its appearance and was required to hold fixation on the target for 300 ms. Typically around 3,000–4,000 trials were collected during each recording session.

To examine the contribution of visual signals to the perisaccadic LFPs, we carried out additional experiments in which the monkeys performed saccades in total darkness (background luminance $<< 0.01$ cd/m^2) without any sparse noise stimulation in the background and a second condition in which the background consisted of static sparse noise patterns. Finally to test the importance of oculomotor signals, we examined another condition in which the monkeys performed "artificial" saccades, consisting of steady fixation while the background visual stimulus shifted diagonally 10 degrees back and forth every second, imitating a shift of the background during an actual saccade. Thus, an artificial saccade toward the RFs would shift the background to the opposite direction of the actual saccade. Since we were limited by the refresh frequency of the projector (75 Hz), the total displacement of the background was completed in 3 frames to correspond to the duration of a regular saccade (40 ms). The background visual stimulus was comprised of static sparse noise patterns.

To examine potential effects of eye position, we performed controls in which the same saccade vector as in the standard experiment (Figure 1D) was executed from different starting positions. Finally, we carried out a control aimed at testing the contribution of the predictability of future saccade target locations. In this experiment the saccade target could change position randomly among three possibilities on each trial, so that the monkey had to wait for its appearance before programming the next saccade. The results of these experiments are shown in Figures S3B and S3C (effects on wave direction) and S3D (effects on wave amplitude).

Data Analysis

Eye Movements

Figure 2A shows typical mean traces of vertical and horizontal eye position around the time of a saccade. Saccade onset was determined as the time when the eye trace left the fixation window. Saccade end was determined as the time following saccade onset when the velocity of the eye trace fell to a value below 10 degrees/s.

Spatial Coherence

Traveling waves can be defined based on spatial synchrony, along with temporal phase differences, at specific frequencies. We detected LFP waves by first calculating the spatial coherence of the LFP. The magnitude of the squared coherence between signals from two different electrodes (x and y) is given by:

$$C_{xy}(f) = \frac{|S_{xy}(f)|^2}{|S_{xx}(f)| * |S_{yy}(f)|}$$

where S_{xy} is the cross-spectrum calculated using Welch's averaged, modified periodogram method, and S_{xx} and S_{yy} are the respective power spectral density estimate (Pesaran et al., 2002). C_{xy} is a measure of the synchrony between two signals as a function of frequency (f); it ranges between 0 and 1. Spatial coherence was calculated from the mean value of C_{xy} across all possible pairs of electrodes and was normalized for each frequency by using spatial coherence from baseline activity periods. In general, spatial coherence for beta LFPs ranged from 0.2 to 0.3.

Wave Detection Algorithm

In order to detect the occurrences of waves in the multielectrode LFP signals and to quantify their parameters, we fitted the beta LFP data to a standard two-dimensional wave equation:

$$u(x,y,t) = A(t) * \sin\left(k_x(t) * x + k_y(t) * y - \omega(t) * t + \varphi(t)\right)$$

where x and y represent coordinates of electrodes on the array, $A(t)$ is the wave amplitude, $k_x(t)$ and $k_y(t)$ are the horizontal and vertical wavelengths respectively, $\omega(t)$ is the angular velocity, and $\varphi(t)$ is the instantaneous phase. The specific approach to detect waves on a planar surface (Symes, 1994) can be thought as a two dimensional variation of a discrete wavelet transform. For a time window of 20 ms, we fitted the equation and computed the parameter estimates $A(t)$, $k_x(t)$, $k_y(t)$, $\omega(t)$ and $\varphi(t)$, with non-linear least-squares using the function lsqcurvefit (Matlab, Mathworks). For every fit corresponding to a specific time window, we acquired one value for each parameter. To track the changes of the parameters through time, we repeated the fit for all different perisaccadic times (−600 to 600 ms relative to the end of the saccade) using a 2 ms step; this procedure yielded a perisaccadic time series for each parameter. To estimate how the parameters changed around the time of each saccade, we normalized the amplitude parameter to its presaccadic (600 to 200 ms before the end of a saccade) value. The onset of a wave was then defined as the time at which the wave amplitude crossed a threshold of 2 standard deviations of the mean presaccadic value and remained above threshold for at least 20 ms (Figure 3).

In order to focus on waves time-locked to the saccades and to increase the signal-to-noise ratio of the LFPs, we computed the mean LFP waveforms across saccades of the same direction. The wave equation was fitted to the averaged data. To identify whether the waves occur at individual trials, we also fitted the wave equation on single trial data.

Preferred Phase

The goal of this analysis was to estimate, for each neuron, the beta LFP phase associated with the strongest spiking activity (Jacobs et al., 2007). For each neuron we calculated the instantaneous phase of the beta LFP on the same channel during periods of visual stimulation with the RF mapping procedure described above. This allowed us to derive phase tuning curves, which related the phase at which a spike occurred. After testing for uniformity using the Rayleigh test (Berens, 2009), the preferred phase was defined as the circular mean of the resulting phase tuning curve.

Calculation of Postsaccadic Peak Response Latency

We estimated postsaccadic latencies for 180 neurons. These neurons were recorded during 10 different saccade experiments, chosen on the basis of a minimum number of saccade trials (around 1,500) that would enable detection of discernible peaks (over 2 standard deviations) in the perisaccadic activity, for more than half of the neurons recorded during the experiment. For each neuron and saccade direction, we calculated a perisaccadic activity histogram, normalized by the neuron's average firing rate 500 to 200 ms before the saccade end; we then computed the latency to peak postsaccadic activity after smoothing the histogram with adaptive regression splines (Wallstrom et al., 2008). In the case of away saccades, the perisaccadic response of many neurons did not have a discernible peak (as evident by the activity of two example neurons and the average histograms shown in Figure S4C), and no peak response latency was reported.

SUPPLEMENTAL INFORMATION

Supplemental Information includes five figures and can be found with this article online at http://dx.doi.org/10.1016/j.neuron.2014.12.043.

ACKNOWLEDGMENTS

We thank Julie Coursol and Cathy Hunt for assistance with animal care and Drs. Julio Martinez-Trujillo and Fernando Chaurand for help with surgical

implantation of the Utah arrays. Dr. Jachin Monteon collected preliminary data, and Drs. Stavros Zanos, Bijan Pesaran, and Jan Churan provided helpful comments on the manuscript. This work was supported by grants from the CIHR (MOP-115178) and NSERC (341534-12) to C.C.P., from FQRNT (No. 149928) to P.J.M., and from the CIHR (MOP-9222) to D.G.

Received: March 20, 2014
Revised: September 2, 2014
Accepted: December 17, 2014
Published: January 15, 2015

REFERENCES

Bartlett, A.M., Ovaysikia, S., Logothetis, N.K., and Hoffman, K.L. (2011). Saccades during object viewing modulate oscillatory phase in the superior temporal sulcus. J. Neurosci. *31*, 18423–18432.

Benucci, A., Frazor, R.A., and Carandini, M. (2007). Standing waves and traveling waves distinguish two circuits in visual cortex. Neuron *55*, 103–117.

Berens, P. (2009). CircStat: A MATLAB toolbox for circular statistics. J. Stat. Softw. *31*, 21.

Buzsaki, G. (2006). Rhythms of the Brain. (New York: Oxford University Press).

Buzsáki, G., and Draguhn, A. (2004). Neuronal oscillations in cortical networks. Science *304*, 1926–1929.

Chen, Y., Geisler, W.S., and Seidemann, E. (2006). Optimal decoding of correlated neural population responses in the primate visual cortex. Nat. Neurosci. *9*, 1412–1420.

Churan, J., Guitton, D., and Pack, C.C. (2011). Context dependence of receptive field remapping in superior colliculus. J. Neurophysiol. *106*, 1862–1874.

Churan, J., Guitton, D., and Pack, C.C. (2012). Spatiotemporal structure of visual receptive fields in macaque superior colliculus. J. Neurophysiol. *108*, 2653–2667.

Destexhe, A., Contreras, D., and Steriade, M. (1999). Spatiotemporal analysis of local field potentials and unit discharges in cat cerebral cortex during natural wake and sleep states. J. Neurosci. *19*, 4595–4608.

Engel, A.K., Kreiter, A.K., König, P., and Singer, W. (1991). Synchronization of oscillatory neuronal responses between striate and extrastriate visual cortical areas of the cat. Proc. Natl. Acad. Sci. USA *88*, 6048–6052.

Ermentrout, G.B., and Kleinfeld, D. (2001). Traveling electrical waves in cortex: insights from phase dynamics and speculation on a computational role. Neuron *29*, 33–44.

Fries, P., Womelsdorf, T., Oostenveld, R., and Desimone, R. (2008). The effects of visual stimulation and selective visual attention on rhythmic neuronal synchronization in macaque area V4. J. Neurosci. *28*, 4823–4835.

Gao, X., Xu, W., Wang, Z., Takagaki, K., Li, B., and Wu, J.Y. (2012). Interactions between two propagating waves in rat visual cortex. Neuroscience *216*, 57–69.

Gattass, R., Sousa, A.P., and Gross, C.G. (1988). Visuotopic organization and extent of V3 and V4 of the macaque. J. Neurosci. *8*, 1831–1845.

Ghose, G.M., and Ts'O, D.Y. (1997). Form processing modules in primate area V4. J. Neurophysiol. *77*, 2191–2196.

Gilbert, C.D., and Wiesel, T.N. (1983). Clustered intrinsic connections in cat visual cortex. J. Neurosci. *3*, 1116–1133.

Heitmann, S., Gong, P., and Breakspear, M. (2012). A computational role for bistability and traveling waves in motor cortex. Front. Comput. Neurosci. *6*, 67.

Henrie, J.A., and Shapley, R. (2005). LFP power spectra in V1 cortex: the graded effect of stimulus contrast. J. Neurophysiol. *94*, 479–490.

Ito, J., Maldonado, P., Singer, W., and Grün, S. (2011). Saccade-related modulations of neuronal excitability support synchrony of visually elicited spikes. Cereb. Cortex *21*, 2482–2497.

Jacobs, J., Kahana, M.J., Ekstrom, A.D., and Fried, I. (2007). Brain oscillations control timing of single-neuron activity in humans. J. Neurosci. *27*, 3839–3844.

Jancke, D., Chavane, F., Naaman, S., and Grinvald, A. (2004). Imaging cortical correlates of illusion in early visual cortex. Nature *428*, 423–426.

Jansen, B.H., and Brandt, M.E. (1991). The effect of the phase of prestimulus alpha activity on the averaged visual evoked response. Electroencephalogr. Clin. Neurophysiol. *80*, 241–250.

Kayser, C., Petkov, C.I., and Logothetis, N.K. (2008). Visual modulation of neurons in auditory cortex. Cereb. Cortex *18*, 1560–1574.

Kleiser, R., Seitz, R.J., and Krekelberg, B. (2004). Neural correlates of saccadic suppression in humans. Curr. Biol. *14*, 386–390.

Knöll, J., Binda, P., Morrone, M.C., and Bremmer, F. (2011). Spatiotemporal profile of peri-saccadic contrast sensitivity. J. Vis. *11*, 15.

Lakatos, P., Shah, A.S., Knuth, K.H., Ulbert, I., Karmos, G., and Schroeder, C.E. (2005). An oscillatory hierarchy controlling neuronal excitability and stimulus processing in the auditory cortex. J. Neurophysiol. *94*, 1904–1911.

Lakatos, P., Chen, C.-M., O'Connell, M.N., Mills, A., and Schroeder, C.E. (2007). Neuronal oscillations and multisensory interaction in primary auditory cortex. Neuron *53*, 279–292.

Lakatos, P., O'Connell, M.N., Barczak, A., Mills, A., Javitt, D.C., and Schroeder, C.E. (2009). The leading sense: supramodal control of neurophysiological context by attention. Neuron *64*, 419–430.

Lee, J., Williford, T., and Maunsell, J.H.R. (2007). Spatial attention and the latency of neuronal responses in macaque area V4. J. Neurosci. *27*, 9632–9637.

Mineault, P.J., Zanos, T.P., and Pack, C.C. (2013). Local field potentials reflect multiple spatial scales in V4. Front. Comput. Neurosci. *7*, 21.

Mitrani, L., Mateeff, S., and Yakimoff, N. (1970). Temporal and spatial characteristics of visual suppression during voluntary saccadic eye movement. Vision Res. *10*, 417–422.

Munoz, D.P., Pélisson, D., and Guitton, D. (1991). Movement of neural activity on the superior colliculus motor map during gaze shifts. Science *251*, 1358–1360.

Nauhaus, I., Busse, L., Carandini, M., and Ringach, D.L. (2009). Stimulus contrast modulates functional connectivity in visual cortex. Nat. Neurosci. *12*, 70–76.

Nikolić, D., Fries, P., and Singer, W. (2013). Gamma oscillations: precise temporal coordination without a metronome. Trends Cogn. Sci. *17*, 54–55.

O'Keefe, J., and Recce, M.L. (1993). Phase relationship between hippocampal place units and the EEG theta rhythm. Hippocampus *3*, 317–330.

Pesaran, B., Pezaris, J.S., Sahani, M., Mitra, P.P., and Andersen, R.A. (2002). Temporal structure in neuronal activity during working memory in macaque parietal cortex. Nat. Neurosci. *5*, 805–811.

Quiroga, R.Q., Nadasdy, Z., and Ben-Shaul, Y. (2004). Unsupervised spike detection and sorting with wavelets and superparamagnetic clustering. Neural Comput. *16*, 1661–1687.

Rajkai, C., Lakatos, P., Chen, C.-M., Pincze, Z., Karmos, G., and Schroeder, C.E. (2008). Transient cortical excitation at the onset of visual fixation. Cereb. Cortex *18*, 200–209.

Ray, S., and Maunsell, J.H.R. (2011). Network rhythms influence the relationship between spike-triggered local field potential and functional connectivity. J. Neurosci. *31*, 12674–12682.

Ross, J., Morrone, M.C., Goldberg, M.E., and Burr, D.C. (2001). Changes in visual perception at the time of saccades. Trends Neurosci. *24*, 113–121.

Rubino, D., Robbins, K.A., and Hatsopoulos, N.G. (2006). Propagating waves mediate information transfer in the motor cortex. Nat. Neurosci. *9*, 1549–1557.

Singer, W., and Gray, C.M. (1995). Visual feature integration and the temporal correlation hypothesis. Annu. Rev. Neurosci. *18*, 555–586.

Sit, Y.F., Chen, Y., Geisler, W.S., Miikkulainen, R., and Seidemann, E. (2009). Complex dynamics of V1 population responses explained by a simple gain-control model. Neuron *64*, 943–956.

Smith, T.J., and Henderson, J.M. (2011). Looking back at Waldo: oculomotor inhibition of return does not prevent return fixations. J. Vis. *11*, 3.

Sompolinsky, H., Golomb, D., and Kleinfeld, D. (1990). Global processing of visual stimuli in a neural network of coupled oscillators. Proc. Natl. Acad. Sci. USA *87*, 7200–7204.

Sundberg, K.A., Mitchell, J.F., Gawne, T.J., and Reynolds, J.H. (2012). Attention influences single unit and local field potential response latencies in visual cortical area V4. J. Neurosci. *32*, 16040–16050.

Symes, W.W. (1994). The plane-wave detection problem. Inverse Probl. *10*, 1361.

Takahashi, K., Saleh, M., Penn, R.D., and Hatsopoulos, N.G. (2011). Propagating waves in human motor cortex. Front. Hum. Neurosci. *5*, 40.

Teichert, T., Klingenhoefer, S., Wachtler, T., and Bremmer, F. (2010). Perisaccadic mislocalization as optimal percept. J. Vis. *10*, 19.

Varela, F., Lachaux, J.-P., Rodriguez, E., and Martinerie, J. (2001). The brainweb: phase synchronization and large-scale integration. Nat. Rev. Neurosci. *2*, 229–239.

Wallstrom, G., Liebner, J., and Kass, R.E. (2008). An implementation of Bayesian Adaptive Regression Splines (BARS) in C with S and R wrappers. J. Stat. Softw. *26*, 1–21.

Wilming, N., Harst, S., Schmidt, N., and König, P. (2013). Saccadic momentum and facilitation of return saccades contribute to an optimal foraging strategy. PLoS Comput. Biol. *9*, e1002871.

Womelsdorf, T., Schoffelen, J.-M., Oostenveld, R., Singer, W., Desimone, R., Engel, A.K., and Fries, P. (2007). Modulation of neuronal interactions through neuronal synchronization. Science *316*, 1609–1612.

Wood, S. (2006). Generalized Additive Models. (Boca Raton, FL: Chapman and Hall/CRC).

Wu, J.-Y., Huang, X., and Zhang, C. (2008). Propagating waves of activity in the neocortex: what they are, what they do. Neuroscientist *14*, 487–502.

Xu, W., Huang, X., Takagaki, K., and Wu, J.Y. (2007). Compression and reflection of visually evoked cortical waves. Neuron *55*, 119–129.

Zanos, T.P., Mineault, P.J., Monteon, J.A., and Pack, C.C. (2011a). Functional connectivity during surround suppression in macaque area V4. In 2011 Annual International Conference of the IEEE Engineering in Medicine and Biology Society, EMBC, pp. 3342–3345.

Zanos, T.P., Mineault, P.J., and Pack, C.C. (2011b). Removal of spurious correlations between spikes and local field potentials. J. Neurophysiol. *105*, 474–486.

Zanos, S., Zanos, T.P., Marmarelis, V.Z., Ojemann, G.A., and Fetz, E.E. (2012). Relationships between spike-free local field potentials and spike timing in human temporal cortex. J. Neurophysiol. *107*, 1808–1821.

Neuron

Supplemental Information

A Sensorimotor Role for Traveling Waves in Primate Visual Cortex

Theodoros P. Zanos, Patrick J. Mineault, Konstantinos T. Nasiotis, Daniel Guitton, and Christopher C. Pack

Figure S1, Related to Figure 2

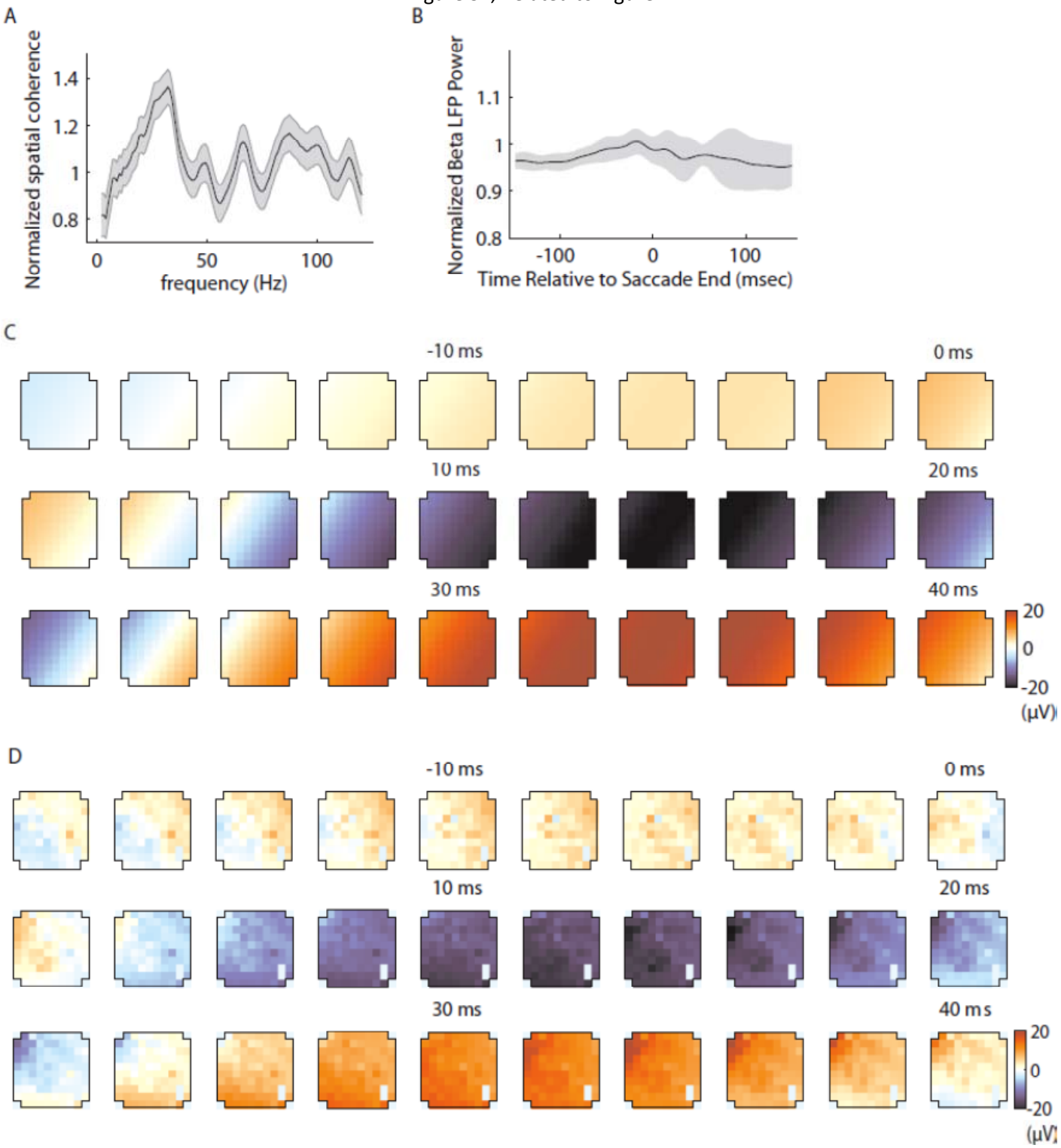

Figure S1, related to Figure 2. Frequency Analysis of the perisaccadic LFPs, reconstructed data from estimated wave parameters and Mean beta LFP activity across all recordings from one monkey.
(A) Normalized spatial coherence for both monkeys and all cases analyzed. **(B)** Perisaccadic beta LFP power for both monkeys and all cases analyzed, normalized to the average beta LFP power value during the complete duration of the experiment. Errors bars represent standard error of the mean. **(C)** Reconstructed beta LFP data using the estimated parameters from the wave detection algorithm. Color scheme as in Figure 2C. **(D)** Mean perisaccadic beta LFP activity at various time points relative to a saccade made toward the RFs, across all recordings from one monkey.

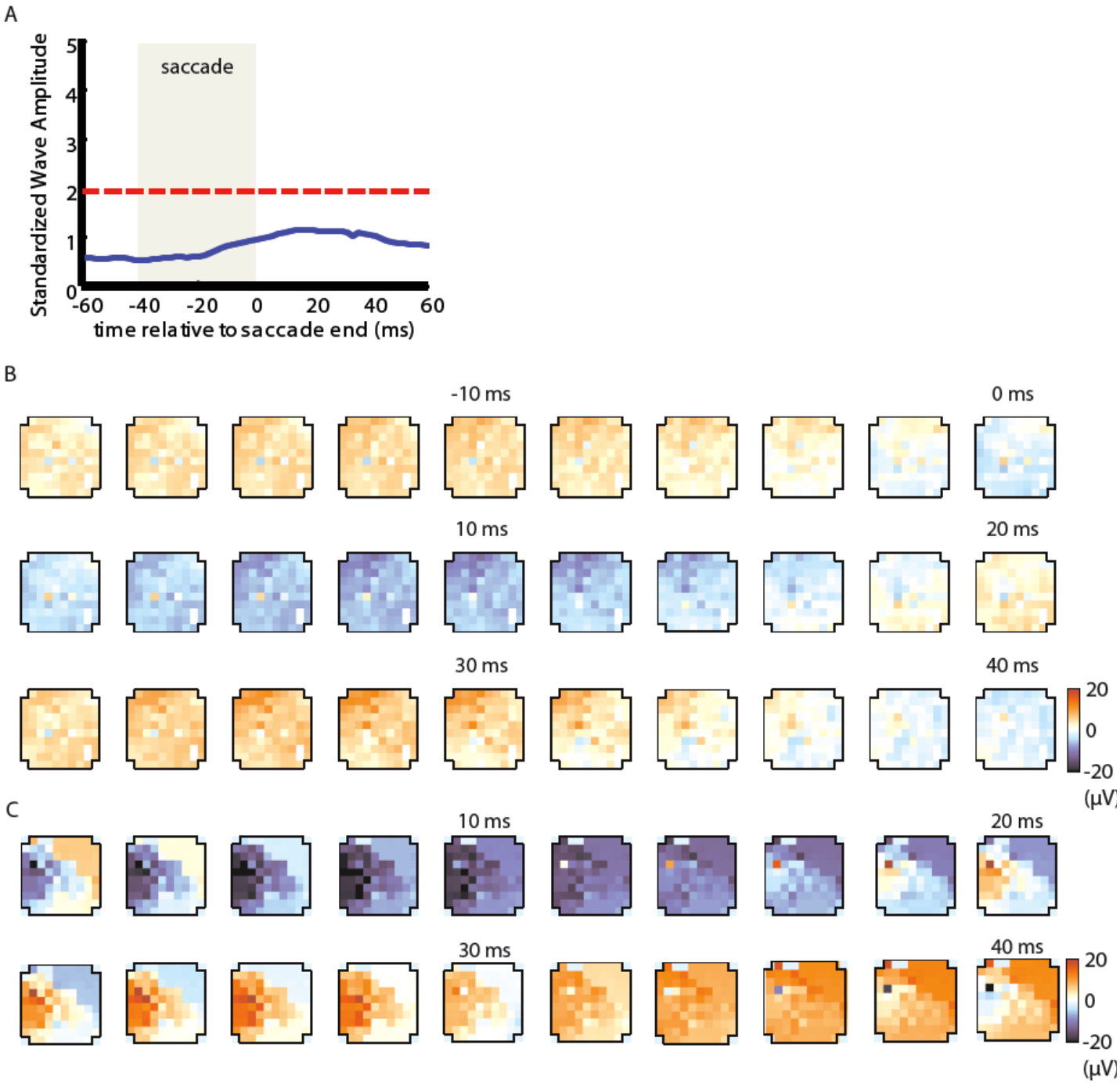

Figure S2, related to Figure 2. Results of the wave detection algorithm for the saccades away from the RFs and Mean perisaccadic beta LFP activity for monkey #2. (A) Temporal evolution of the amplitude of the beta LFP activity illustrated in Figure S2B for saccades away from the RFs, as estimated by the wave detection algorithm. The red dotted line indicates the wave detection threshold. **(B)** Snapshots of post-saccadic averaged Beta LFP signals for saccades away from the RFs. Each snapshot depicts activity every 2 ms. Time values are relative to the end of the saccade. Color scheme as in Figure 2C. **(C)** Mean perisaccadic beta LFP activity at various time points relative to a saccade made toward the RFs, recorded on the array on the second monkey. The orientation of the array with respect to the retinotopic gradient is different in this monkey, due to the surgical placement of the array and it was accounted for in all analyses.

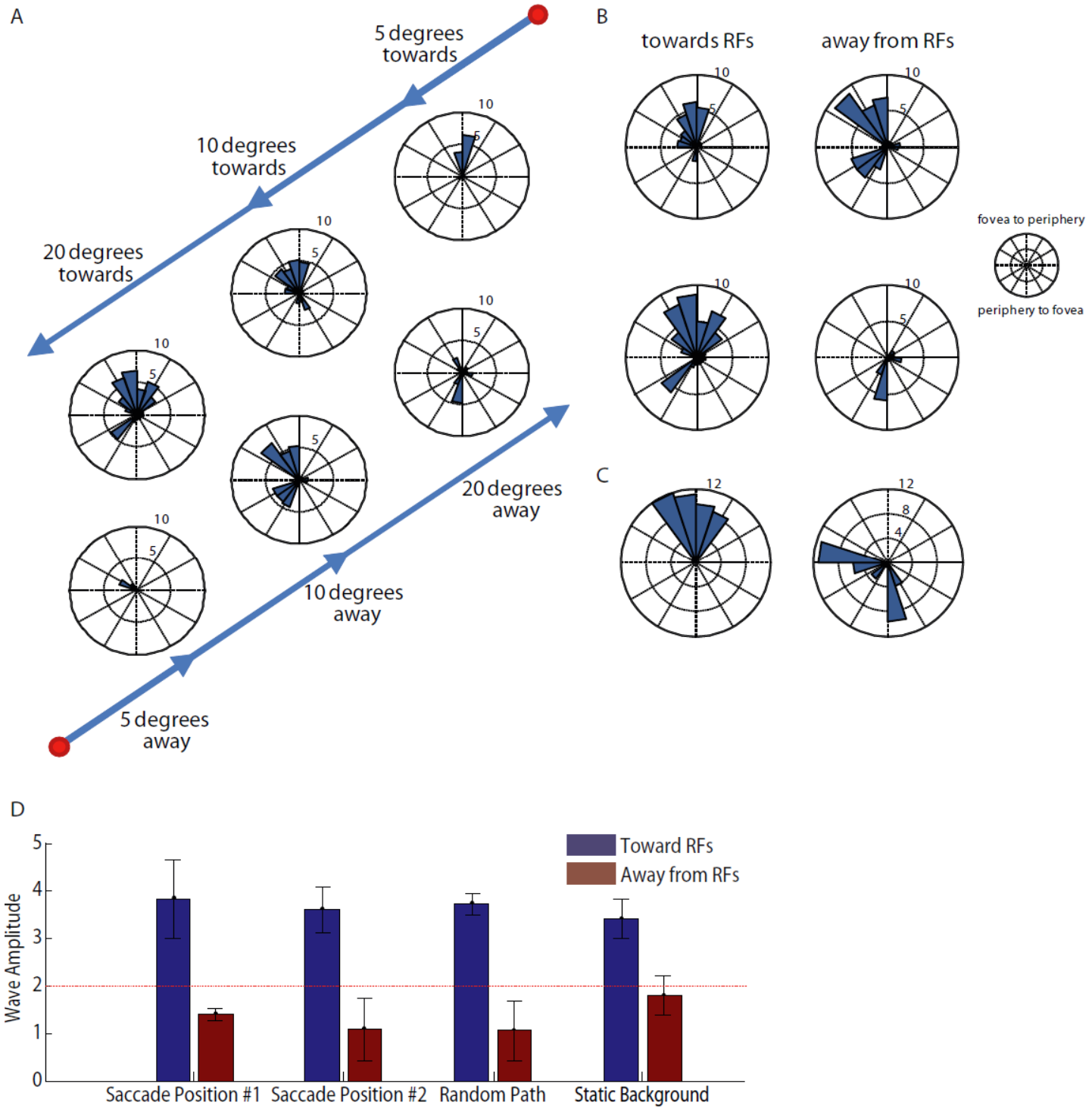

Figure S3, related to Figure 4. Properties of traveling waves in V4 for control experiments.
(A) Retinotopic wave directions for three saccade sizes, for saccades towards (top row) and away (bottom row) from the RFs. **(B)** Retinotopic wave directions for saccades with different starting positions. The upper panel corresponds to saccades beginning at x, y position (4^o,4^o) and ending at (-4^o,-4^o). The middle panel to saccades from (4^o,19^o) to (-4^o,5^o) – coordinates in visual degrees from the center of the visual field. **(C)** Retinotopic wave directions for diagonal saccades against static background stimulus. **(D)** Mean standardized (z-scored) amplitude values derived from the wave algorithm for control experiments involving different saccade positions, different saccade paths, and a static background.

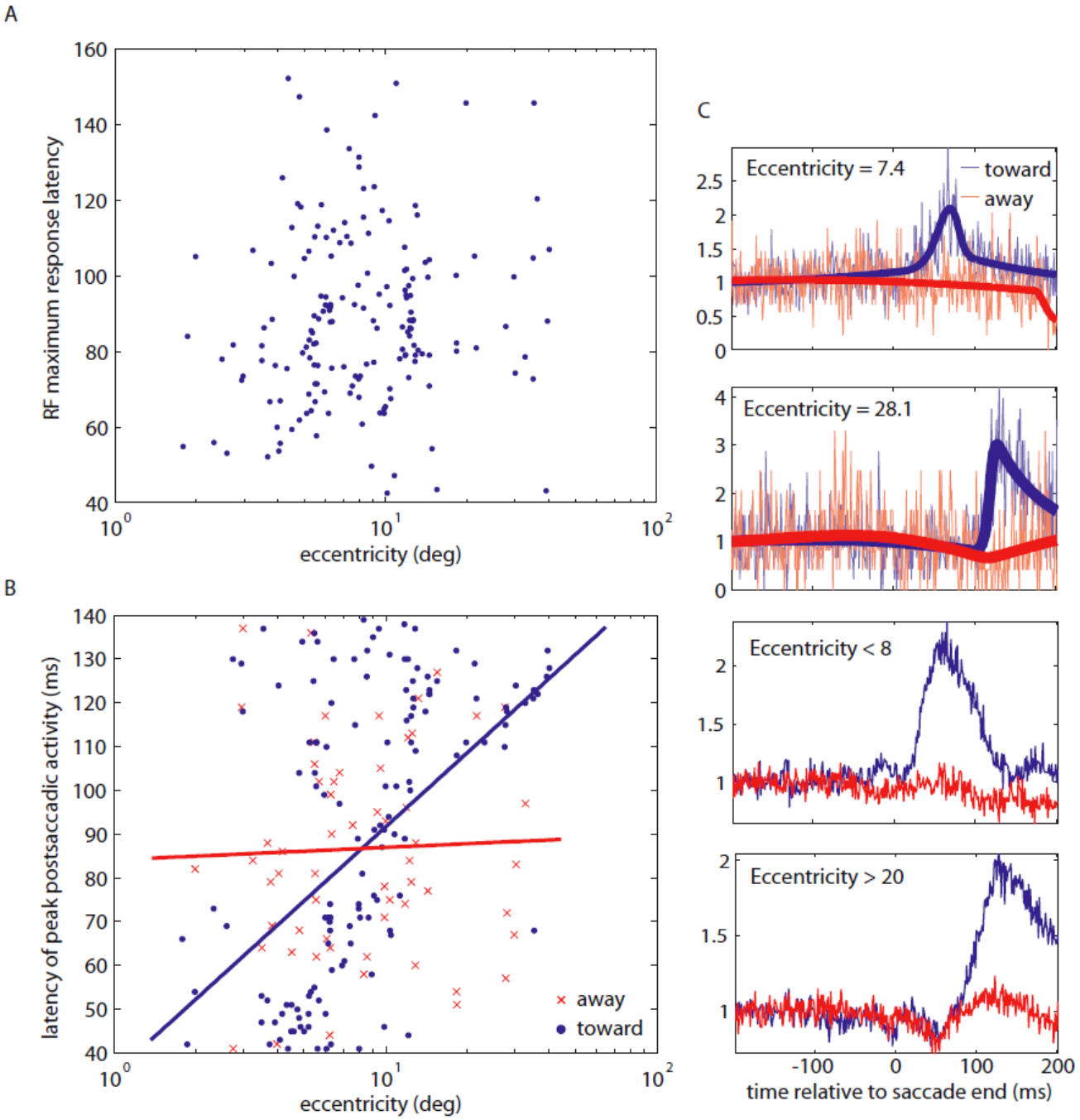

Figure S4, related to Figure 7. Response profiles of V4 neurons. (A) Maximum response latency of V4 neurons during fixation, plotted against their eccentricity. **(B)** Latency of the increase of postsaccadic sensitivity for V4 neurons with different positions along the retinotopic map, for saccades toward the RFs (blue dots) and away from the RFs (red Xs). Lines denote regression lines for the saccades toward (blue) and away (red) from the RFs. **(C)** Perisaccadic modulation of the activity of two example neurons, a parafoveal (upper panel) and a peripheral (lower panel), to the sparse noise background visual stimulus and average perisaccadic histograms for all foveal (less than 8 visual degrees) and peripheral (more than 20 degrees). Perisaccadic response histograms for saccades toward the RFs (blue curve) and away from the RFs (red curve). Solid lines indicate spline fits to the raw data.

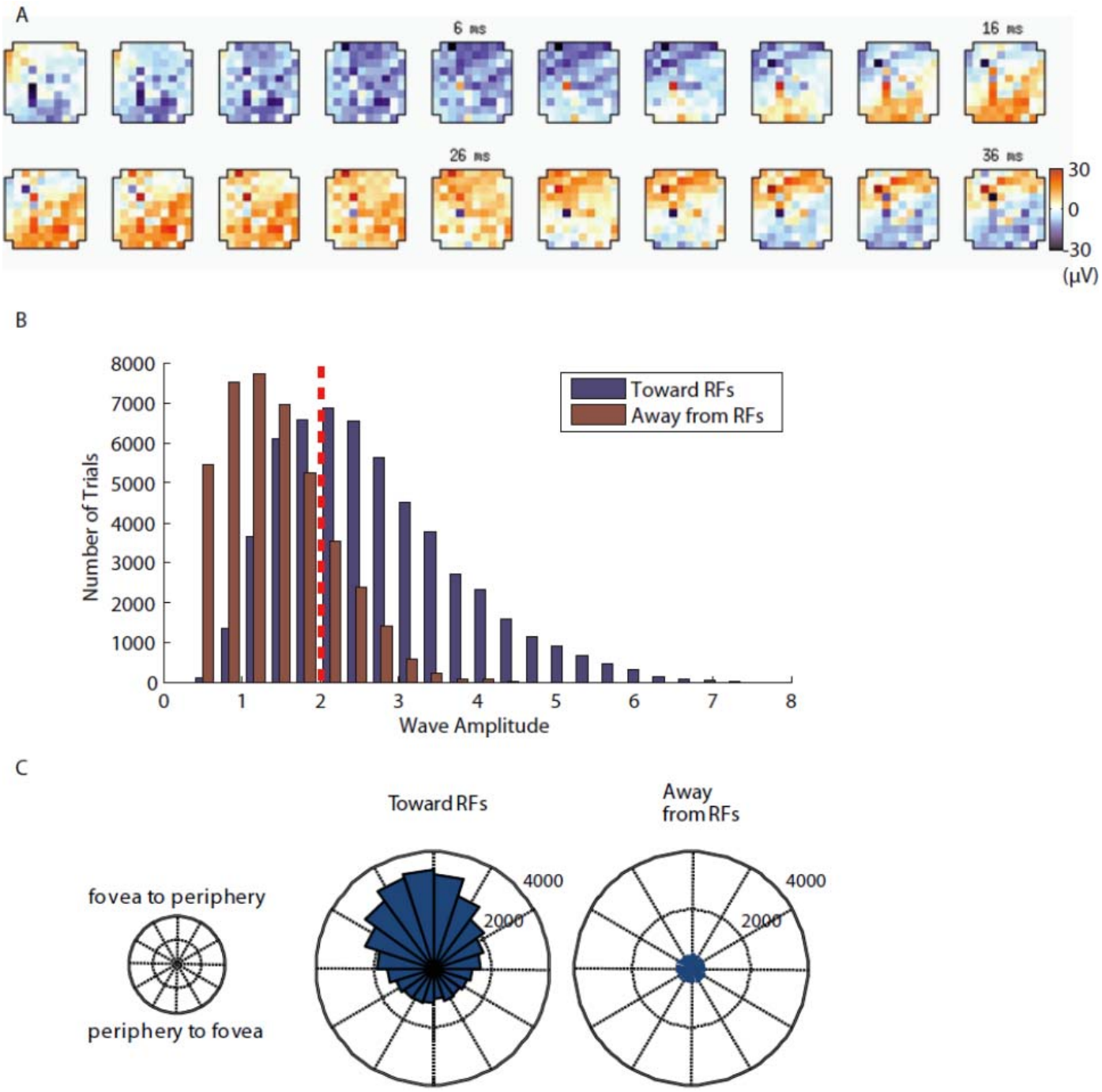

Figure S5, related to Figure 3. Results of trial by trial analysis. Statistically significant waves were present in 67.3% of toward saccade trials, for all saccade experiments in both monkeys (a total of 37472 out of 55647 toward the RFs saccade trials). For saccades away from the RFs, waves were present in 20.6% (8283 out of 40155) of the trials. **(A)** Example of raw beta LFP activity from a single "toward saccade" trial. **(B)** Average amplitude histograms of all waves detected for both saccade directions. **(C)** Average direction histograms of all waves detected for both saccade directions.